Dephasing of coherences between σ^+ and σ^- exciton states in a ZnSe single quantum well

H. P. Wagner and S. Tripathy
Department of Physics, University of Cincinnati, Cincinnati, Ohio 45221-0011, USA
(Received 18 September 2003; revised manuscript received 19 December 2003; published 18 March 2004)

We investigate interband coherences as well as coherences between σ^+ and σ^- exciton states in a 10 nm thick ZnSe/ZnMgSe single quantum well by spectrally resolved three-pulse degenerate four-wave mixing using circularly polarized 100 fs pulses. Polarization and intensity dependent measurements are performed to identify the coherent processes responsible for the nonlinear signal into the $\mathbf{k}_3+\mathbf{k}_2-\mathbf{k}_1$ direction and to study the influence of Coulomb scattering on the dephasing rates. The experiments reveal nearly equal zero-density dephasing rates for coherences between σ^+ and σ^- heavy- and/or light-hole exciton states as compared to the dephasing rate of the interband coherence between these states and the ground state. The measurements also demonstrate that exciton–exciton scattering destroys the phase coherence between heavy- and light-hole excitons about three times more effectively than the coherence between σ^+ and σ^- heavy-hole excitons. The characteristic features of the experimental results are explained and reproduced by numerical calculations of the optical Bloch equations for a ten-level model including excitation induced dephasing.

DOI: 10.1103/PhysRevB.69.125325 PACS number(s): 71.35.−y, 71.55.Gs, 42.50.Md

INTRODUCTION

The technique of degenerate four-wave mixing (FWM) represents a powerful tool to study fundamental coherent transient phenomena in bulk semiconductors and quantum well (QW) structures. In particular, FWM provides an experimental approach for the investigation of quantum beat phenomena,[1–3] scattering processes of excitons with free carriers,[4,5] with excitons[6–9] and with phonons.[9–11] A general theoretical approach to analyze these coherent optical phenomena is based on the semiconductor Bloch equations (SBE),[12] which consider the fermionic nature and the Coulomb interaction of carriers in a semiconductor. However, under certain excitation conditions the important mechanisms can be obtained also if the complexity of the SBE is simplified by phenomenological multilevel models, essentially representing extended optical Bloch equations (OBE). These models consider e.g., local-field effects (LFE),[13] excitation-induced dephasing (EID),[14–16] and biexciton formation (BIF).[17–19] The off-diagonal elements of the density matrices in these models describe the coherence between exciton states, which decays with their characteristic relaxation time. Most investigations concentrate on interband coherences between the ground state and the heavy-hole X_h or light-hole X_l exciton states or between the ground state and two-exciton states (biexciton transitions) using standard two-pulse degenerate four-wave mixing. Much less studied, however, are coherences between two heavy-hole or two light-hole excitons of opposite spin and between heavy-hole and light-hole excitons with opposite or equal spin,[20,21] which are generated in a two-photon coherent process. Their interactions with excitons, phonons and impurities may differ from that of interband coherences leading to different decay rates of both types of coherent excitations.[21] Coherences between two excitons will be called interexciton coherences in what follows.

In this paper, we investigate interband and interexciton coherences in a ZnSe single quantum well by applying polarization dependent three-pulse degenerate four-wave mixing experiments. Since ZnSe possesses an exciton oscillator strength, which is about 10 times higher than that of GaAs, this SQW structure is well suited for the study of the mentioned coherent phenomena. The higher biexciton binding energy in II–VI semiconductors compared to III–V semiconductors also enables a spectral isolation of the heavy-hole biexciton XX_h transition as well as of the mixed heavy-hole–light-hole biexciton XX_m transition.[19,22] The zero-density dephasing rates as well as exciton–exciton scattering parameters for different interband and interexciton exciton coherences are obtained by intensity dependent measurements. For a more detailed understanding of the different FWM processes, the optical Bloch equations of a 10-level system including excitation induced dephasing (EID) have been solved numerically and the calculations are compared with our experimental results.

EXPERIMENTAL DETAILS

The investigated ZnSe single quantum wells were pseudomorphically grown on (001) oriented GaAs substrate by molecular beam epitaxy (MBE). The structures include a ZnSe quantum well of 10 nm width sandwiched between two 25 nm thick $Zn_{0.90}Mg_{0.1}Se$ barriers defining a type-I quantum well structure. A detailed description of the growth and a sample characterization is given in Ref. 23. A frequency doubled mode locked Ti–sapphire laser providing ultrashort pulses of spectral width of 22 meV at a repetition rate of 82 MHz was used to excite the sample. The temporal width of the frequency doubled pulses was determined to 103 ± 4 fs using an autocorrelation technique that is based on two-photon-absorption in a SiC photodiode. The three-beam four-wave mixing experiments, which involve three excitation pulses $\mathbf{k}_1$, $\mathbf{k}_2$, and $\mathbf{k}_3$, have been performed in the backscattering geometry with the sample mounted in a helium cryostat at a temperature of 55 K. In the experiments the delay time between $\mathbf{k}_1$ and $\mathbf{k}_2$ was kept to zero ($\tau_{12}=t_2-t_1\approx0$) while the time delay $\tau_{13}=t_3-t_1=\tau$ was varied between pulses $\mathbf{k}_1$ and $\mathbf{k}_3$. The zero delay between pulses $\mathbf{k}_1$ and $\mathbf{k}_2$ as well as between $\mathbf{k}_1$ and $\mathbf{k}_3$ has been determined by maximum contrast of the light interference pattern appearing

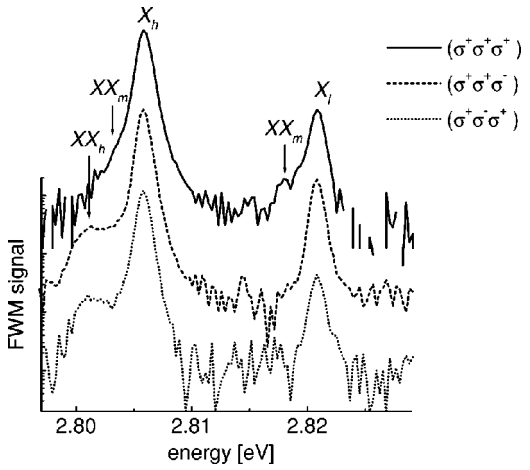

FIG. 1. Spectrally resolved three-beam FWM signals of a 10 nm thick ZnSe SQW into $\mathbf{k}_3+\mathbf{k}_2-\mathbf{k}_1$ direction for polarization configurations $(\sigma^+\sigma^+\sigma^+)$, $(\sigma^+\sigma^+\sigma^-)$, and $(\sigma^+\sigma^-\sigma^+)$ at 55 K. The spectra were taken at a delay time $\tau=-0.55$ ps. The excitation was centered at 2.808 eV, the intensity of pulses $\mathbf{k}_1$ and $\mathbf{k}_2$ was 1.3 MW cm^{-2} and of pulse $\mathbf{k}_3$ was 0.3 MW cm^{-2}. The exciton (X_h, X_l) and biexciton transitions (XX_h, XX_m) are labeled.

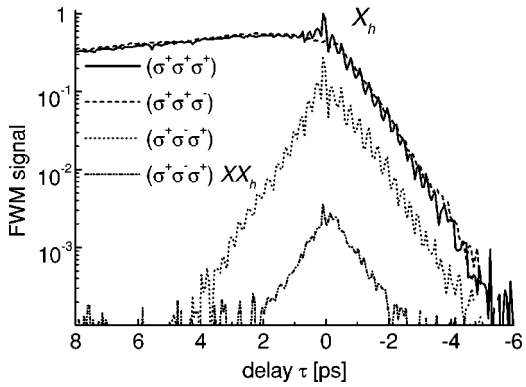

FIG. 2. FWM traces into $\mathbf{k}_3+\mathbf{k}_2-\mathbf{k}_1$ direction at the spectral position of the heavy-hole X_h exciton transition for polarization configurations $(\sigma^+\sigma^+\sigma^+)$, $(\sigma^+\sigma^+\sigma^-)$, and $(\sigma^+\sigma^-\sigma^+)$ and at the heavy-hole biexciton induced transition XX_h for configuration $(\sigma^+\sigma^-\sigma^+)$ at 55 K. The intensity of pulses $\mathbf{k}_1$ and $\mathbf{k}_2$ was set to 1.3 MW cm^{-2}, the intensity of pulse $\mathbf{k}_3$ was 0.3 MW cm^{-2}.

on the sample surface during temporal overlap of the pulses. The $1/e^2$ focus diameter of the pulses on the sample was 100 μm. The time integrated and spectrally resolved four wave mixing signal was detected in direction $\mathbf{k}_3+\mathbf{k}_2-\mathbf{k}_1$ by a combination of a spectrometer and an optical multichannel analyzer. The experiments have been performed for various polarization configurations of the three incident pulses. In the present discussion we use the notation $(\sigma^+\sigma^+\sigma^+)$, $(\sigma^+\sigma^+\sigma^-)$, and $(\sigma^+\sigma^-\sigma^+)$ where the first, second, and third symbol in the parentheses indicates the polarization of the $\mathbf{k}_1$, $\mathbf{k}_2$, and $\mathbf{k}_3$ pulse, respectively.

EXPERIMENTAL RESULTS

In the performed three-beam four-wave mixing experiments a positive delay ($\tau>0$) refers to the case where pulse $\mathbf{k}_3$ arrives last whereas a negative delay ($\tau<0$) refers to pulse $\mathbf{k}_3$ arriving first. Figure 1 shows the spectrally resolved FWM signal in the $\mathbf{k}_3+\mathbf{k}_2-\mathbf{k}_1$ direction obtained from the 10 nm ZnSe SQW at a delay time $\tau=-0.55$ ps for configurations $(\sigma^+\sigma^+\sigma^+)$, $(\sigma^+\sigma^+\sigma^-)$, and $(\sigma^+\sigma^-\sigma^+)$. The intensity of pulses $\mathbf{k}_1$ and $\mathbf{k}_2$ together was 1.3 MW cm^{-2} and the intensity of the third pulse $\mathbf{k}_3$ was 0.3 MW cm^{-2}. The center of the 22 meV broad excitation pulse was set to 2.808 eV, in order to avoid continuum contributions and predominantly excite the $11H$ X_h heavy-hole exciton at 2.806 eV and weakly excite the light-hole $11L$ X_l exciton transition at 2.821 eV. In addition the heavy-hole biexciton induced signal XX_h at (2.806 eV$-\Delta_h$) (Ref. 19) and the mixed heavy-light-hole biexciton induced signals XX_m at (2.806 eV$-\Delta_m$) and (2.821 eV$-\Delta_m$) (Ref. 22) are observed, both being identified from their polarization dependence as described in the next paragraph. In the parentheses $\Delta_h=4.8$ meV is the binding energy of the heavy–heavy-hole biexciton, $\Delta_m=2.8$ meV refers to the binding energy of the mixed heavy–light-hole biexciton. The weak $12H$ heavy-hole exciton transition visible at 2.815 eV was not considered in the following treatment. Two pulse four-wave mixing experiments[19,22] further indicate that the exciton transitions are nearly homogeneously broadened in this ZnSe SQW.

The FWM responses as a function of delay time τ for configurations $(\sigma^+\sigma^+\sigma^+)$, $(\sigma^+\sigma^+\sigma^-)$, and $(\sigma^+\sigma^-\sigma^+)$ at the energetic position of the X_h transition and for the $(\sigma^+\sigma^-\sigma^+)$ configuration at the biexciton induced XX_h transition are displayed in Fig. 2. For negative delay time ($\tau<0$), pulse $\mathbf{k}_3$ builds up an exciton polarization, which, together with the subsequent pulses $\mathbf{k}_1$ and $\mathbf{k}_2$ leads to the generation of a FWM signal into the direction of $\mathbf{k}_3+\mathbf{k}_2-\mathbf{k}_1$. In all configurations the observed FWM signal decays with the dephasing rate of the interband exciton polarization. While clear quantum beats between heavy-X_h and light-hole X_l excitons with a period $\Delta\tau\approx270$ fs (corresponding to an energy splitting of $\Delta E_{hl}=h/\Delta\tau\approx15$ meV) are observed in $(\sigma^+\sigma^+\sigma^+)$ and $(\sigma^+\sigma^-\sigma^+)$ configuration, no oscillations are visible in $(\sigma^+\sigma^+\sigma^-)$ configuration. The observed quantum beats reveal a constant oscillation amplitude indicating very similar X_h and X_l single exciton interband dephasing times.

For positive delay time ($\tau>0$) in configurations $(\sigma^+\sigma^+\sigma^+)$ and $(\sigma^+\sigma^+\sigma^-)$ pulses $\mathbf{k}_1$ and $\mathbf{k}_2$ have the same circular polarization so that an exciton population grating with grating vector $\mathbf{k}_2-\mathbf{k}_1$ is generated. The electric field of the delayed pulse $\mathbf{k}_3$ (with same or different circular polarization) generates a nonlinear FWM signal into direction $\mathbf{k}_3+\mathbf{k}_2-\mathbf{k}_1$. The FWM signal persists as long as the grating exits i.e., the signal decays with the inverse of the exciton lifetime T_1 and decreases also due to the diffusion of excitons within the population grating leading to a reduced contrast of the population grating with increasing delay time τ.[24] Only in the $(\sigma^+\sigma^+\sigma^+)$ configuration X_h–X_l quantum beats with damped oscillating amplitude are observed. Furthermore the FWM signal in $(\sigma^+\sigma^+\sigma^+)$ configuration shows an increase near zero delay, which is not observed in the $(\sigma^+\sigma^+\sigma^-)$ configuration. As outlined in the next paragraph this behavior is explained by excitation induced dephasing

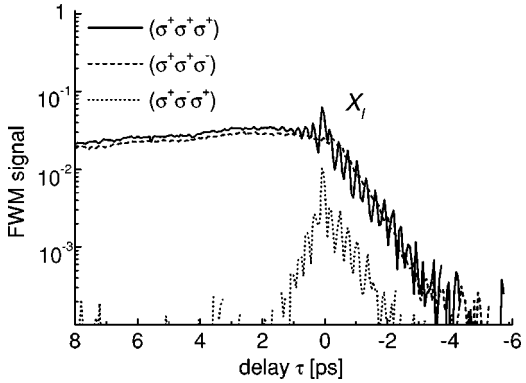

FIG. 3. FWM traces into $\mathbf{k}_3+\mathbf{k}_2-\mathbf{k}_1$ direction at the spectral position of the light-hole X_l exciton transition for polarization configurations $(\sigma^+\sigma^+\sigma^+)$, $(\sigma^+\sigma^+\sigma^-)$, and $(\sigma^+\sigma^-\sigma^+)$ at 55 K. The intensity of pulses $\mathbf{k}_1$ and $\mathbf{k}_2$ was set to 1.3 MW cm^{-2}, the intensity of pulse $\mathbf{k}_3$ was 0.3 MW cm^{-2}.

(EID) which is present for $(\sigma^+\sigma^+\sigma^+)$ polarized fields but is inactive in the $(\sigma^+\sigma^+\sigma^-)$ configuration.

The FWM signal observed in the $(\sigma^+\sigma^-\sigma^+)$ configuration for $\tau>0$ behaves significantly different. In this case pulses $\mathbf{k}_1$ and $\mathbf{k}_2$ cannot create a population grating because they act on different σ^+ and σ^- exciton transitions. Instead they create an interexciton coherence between σ^+ and σ^- excitons that has a structure of an orientational grating with momentum $\mathbf{k}_2-\mathbf{k}_1$. Again together with $\mathbf{k}_3$ a nonlinear FWM signal is generated into direction $\mathbf{k}_3+\mathbf{k}_2-\mathbf{k}_1$. The nonlinear signal decays with the same rate as the coherence between two σ^+ and σ^- excitons is lost, thus enabling the determination of the not otherwise accessible interexciton exciton dephasing time. A closer look to the FWM trace, however, shows that the decay cannot be fitted with a single exponential function. Also the X_h–X_l beating clearly observed in this configuration shows a slight damping for positive delay. In the following paragraph these observations are explained by the decoherence between X_h and X_l excitons of opposite spin as well as by EID both contributing to the FWM signal at resonance X_h. The FWM trace at the biexciton induced XX_h transition is (up to third order perturbation) neither affected by the X_h–X_l interexciton decoherence nor by EID so that the X_h interexciton dephasing time can be directly evaluated from this signal.

The FWM traces at the energetic position of the X_l exciton (see Fig. 3) show very similar features as observed at the X_h transition energy. In the $(\sigma^+\sigma^-\sigma^+)$ configuration for $\tau>0$ the decay rate of the FWM signal is faster as compared to the decay rate of the FWM signal at the spectral position of X_h indicating a faster loss of the coherence between two σ^+ and σ^- light-hole excitons X_l as well as between X_h and X_l excitons of different spin.

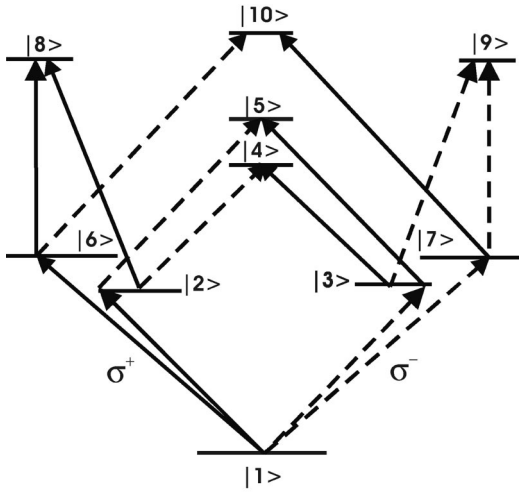

FIG. 4. Ten-level scheme describing a system of interacting heavy-hole X_h and light-hole X_l exciton with ground level $|1\rangle$, σ^+ and σ^- X_h heavy-hole (levels $|2\rangle$ and $|3\rangle$), X_l light-hole excitons (levels $|6\rangle$ and $|7\rangle$), heavy-hole biexcitons XX_h and biexciton continuum (levels $|4\rangle$ and $|5\rangle$), mixed biexcitons XX_m (levels $|8\rangle$ and $|9\rangle$) and a light-hole biexciton continuum (level $|10\rangle$). The arrows represent the optical transitions (full line σ^+ transition, dashed line σ^- transition) and their selection rules.

THEORETICAL MODEL

For a more quantitative understanding of the experimental data we have modeled the FWM response by solving the optical Bloch equations (OBE) of a 10-level system up to third order in the external fields for δ-shaped laser pulses. The 10-level model (see Fig. 4) with the ground level $|1\rangle$ initially populated takes into account the interaction of σ^+ and σ^- X_h heavy-hole (levels $|2\rangle$ and $|3\rangle$) and X_l light-hole excitons (levels $|6\rangle$ and $|7\rangle$) and also allows for the formation of bound heavy-hole biexcitons XX_h and biexciton continuum (levels $|4\rangle$ and $|5\rangle$). Furthermore the formation of mixed biexcitons XX_m (levels $|8\rangle$ and $|9\rangle$) as well as of a light-hole biexciton continuum (level $|10\rangle$) is introduced into this model. The corresponding OBE are further extended to encompass EID, as discussed in Ref. 16. Local field effects (LFE) have not been considered since they are less important in ZnSe quantum wells as shown in previous two-beam FWM experiments.[19] After Fourier transformation the third-order polarization into $\mathbf{k}_3+\mathbf{k}_2-\mathbf{k}_1$ direction for negative $(\tau<0)$ and positive $(\tau>0)$ delay reads

$$P^{(3)}_{\mathbf{k}_3+\mathbf{k}_2-\mathbf{k}_1}(\omega,\tau<0)=\frac{N}{\hbar^3}\Theta(-\tau)\sum_{s,s',t}\left[\frac{\boldsymbol{\mu}^*_{sg}}{(\omega-\tilde{\Omega}_{sg})}[(\boldsymbol{\mu}_{s'g}\cdot\mathbf{e}_2)(\boldsymbol{\mu}^*_{s'g}\cdot\mathbf{e}^*_1)(\boldsymbol{\mu}_{sg}\cdot\mathbf{e}_3)\exp(i\Omega_{sg}\tau)+[(\boldsymbol{\mu}^*_{ts}\cdot\mathbf{e}^*_1)(\boldsymbol{\mu}_{ts'}\cdot\mathbf{e}_2)\right.$$

$$\left.+(\boldsymbol{\mu}_{sg}\cdot\mathbf{e}_2)(\boldsymbol{\mu}^*_{s'g}\cdot\mathbf{e}^*_1)](\boldsymbol{\mu}_{s'g}\cdot\mathbf{e}_3)\exp(i\Omega_{s'g}\tau)]-\frac{2\boldsymbol{\mu}^*_{ts}}{(\omega-\tilde{\Omega}_{ts})}(\boldsymbol{\mu}_{ts'}\cdot\mathbf{e}_2)(\boldsymbol{\mu}^*_{sg}\cdot\mathbf{e}^*_1)(\boldsymbol{\mu}_{s'g}\cdot\mathbf{e}_3)\exp(i\Omega_{s'g}\tau)\right.$$

$$+iN\beta\frac{\boldsymbol{\mu}_{sg}^*}{(\omega-\tilde{\Omega}_{sg})^2}[2(\boldsymbol{\mu}_{sg}\cdot\mathbf{e}_3)(\boldsymbol{\mu}_{s'g}\cdot\mathbf{e}_2)(\boldsymbol{\mu}_{s'g}^*\cdot\mathbf{e}_1^*)\exp(i\Omega_{sg}\tau)$$

$$+(\boldsymbol{\mu}_{s'g}\cdot\mathbf{e}_3)(\boldsymbol{\mu}_{sg}\cdot\mathbf{e}_2)(\boldsymbol{\mu}_{s'g}^*\cdot\mathbf{e}_1^*)\exp(i\Omega_{s'g}\tau)], \tag{1}$$

$$P^{(3)}_{\mathbf{k}_3+\mathbf{k}_2-\mathbf{k}_1}(\omega,\tau>0)=\frac{N}{\hbar^3}\Theta(\tau)\exp(i\omega\tau)\sum_{s,s',t}\left[\frac{2\boldsymbol{\mu}_{sg}^*}{(\omega-\tilde{\Omega}_{sg})}\right.$$

$$\times\left[(\boldsymbol{\mu}_{sg}\cdot\mathbf{e}_3)(\boldsymbol{\mu}_{s'g}\cdot\mathbf{e}_2)(\boldsymbol{\mu}_{s'g}^*\cdot\mathbf{e}_1^*)\exp\left(-\frac{\tau}{T_c}\right)+(\boldsymbol{\mu}_{s'g}\cdot\mathbf{e}_3)(\boldsymbol{\mu}_{s'g}^*\cdot\mathbf{e}_1^*)(\boldsymbol{\mu}_{sg}\cdot\mathbf{e}_2)\exp(-i\Omega_{ss'}\tau)\right]$$

$$-\frac{2\boldsymbol{\mu}_{ts}^*}{(\omega-\tilde{\Omega}_{ts})}(\boldsymbol{\mu}_{ts'}\cdot\mathbf{e}_3)(\boldsymbol{\mu}_{s'g}\cdot\mathbf{e}_2)(\boldsymbol{\mu}_{sg}^*\cdot\mathbf{e}_1^*)\exp(-i\Omega_{s's}\tau)+iN\beta\exp\left(-\frac{\tau}{T_c}\right)\frac{\boldsymbol{\mu}_{sg}^*}{(\omega-\tilde{\Omega}_{sg})^2}[2(\boldsymbol{\mu}_{sg}\cdot\mathbf{e}_3)$$

$$\left.\times(\boldsymbol{\mu}_{s'g}\cdot\mathbf{e}_2)(\boldsymbol{\mu}_{s'g}^*\cdot\mathbf{e}_1^*)+\exp(-i\Omega_{sg}\tau)(\boldsymbol{\mu}_{sg}\cdot\mathbf{e}_2)(\boldsymbol{\mu}_{s'g}\cdot\mathbf{e}_3)(\boldsymbol{\mu}_{s'g}^*\cdot\mathbf{e}_1^*)\exp(i\Omega_{s'g}^*\tau)]\right]. \tag{2}$$

In Eqs. (1) and (2), $\mathbf{e}_j$ denotes the polarization unit vectors of the σ^+ and σ^- polarized laser pulses with $\boldsymbol{\sigma}^{\pm}=2^{-0.5}(1,\mp i)$ in Jones notation and $j=1,2,3$ corresponding to the three laser pulses. The indices s and s' correspond to the single exciton states ($|2\rangle$, $|3\rangle$, $|6\rangle$, $|7\rangle$) whereas t refers to the two-exciton states ($|4\rangle$, $|5\rangle$, $|8\rangle$, $|9\rangle$, $|10\rangle$, g being the ground state $|1\rangle$. The optical matrix elements from ground state g to states s are $\boldsymbol{\mu}_{gs}$ where $\boldsymbol{\mu}_{gs}=\mu_{gs}\boldsymbol{\sigma}^+$ or $\mu_{gs}\boldsymbol{\sigma}^-$ where μ_{gs} accounts for the magnitude of the dipole transitions. Furthermore we have used the following abbreviations:

$$\Omega_{sg}=\omega_{sg}-i\gamma_{sg}=\omega_{sg}-i(\gamma_{sg}^0+\beta_{sg}N_3),$$

$$\Omega_{s's}=\omega_{s's}-i\gamma_{s's}=\omega_{s's}-i(\gamma_{s's}^0+\beta_{s's}(N_1+N_2)),$$

$$\tilde{\Omega}_{sg}=\Omega_{sg}-i\beta_{sg}(N_1+N_2),$$

$$\tilde{\Omega}_{ts}=\omega_{ts}-i(\gamma_{ts}^0+\beta_{ts}(N_1+N_2+N_3)). \tag{3}$$

The dephasing rates γ_{sg} are given by $\gamma_{sg}=(T_{sg})^{-1}$, where T_{sg} are the interband dephasing times of different X_h and X_l exciton to ground transitions. For $s\neq s'$ the interexciton dephasing rate $\gamma_{s's}$ is given by $\gamma_{s's}=(T_{s's})^{-1}$. The time constant $T_{s's}$ describes the loss of coherence between two X_h, two X_l and X_h-X_l exciton states with different spin (T_{32}, T_{76}, T_{63},T_{72}, respectively) as well as between X_h-X_l exciton states with equal spin (T_{62},T_{73}). For $s=s'$ the decay rate of the exciton population grating is given by $\gamma_{s's}=(T_c)^{-1}$. T_c is a combined time constant taking into account the exciton lifetime as well as the exciton diffusion inside the population grating. The quantities ω_{sg}, $\omega_{s's}$, ω_{ts} are the angular frequency between states g, s, s' and t, N is the total density of the exciton system. γ_{sg}^0 and $\gamma_{s's}^0$ denote the dephasing rates at zero exciton density and β_{sg} and $\beta_{s's}$,β_{ts} are the exciton–exciton scattering parameters taking into account an increased dephasing rate of various transitions with exciton densities N_1, N_2, and N_3 created by the three-laser pulses $\mathbf{k}_1$, $\mathbf{k}_2$, and $\mathbf{k}_3$, respectively. The exciton–exciton scattering parameter $\beta=\beta_{sg}$ is also responsible for the EID terms in Eqs. (1) and (2).

Numerical calculations have been performed for configurations $(\sigma^+\sigma^+\sigma^+)$, $(\sigma^+\sigma^+\sigma^-)$, and $(\sigma^+\sigma^-\sigma^+)$. The energetic positions of exciton and biexciton induced transitions were taken from the experimental FWM spectra. From the FWM traces we evaluated the combined lifetime T_c to $T_c=35$ ps as well as the interband dephasing rates $\gamma_{21}=\gamma_{31}=0.75\ \mathrm{ps}^{-1}$ and $\gamma_{61}=\gamma_{71}=0.75\ \mathrm{ps}^{-1}$. The interexciton dephasing rate $\gamma_{32}=0.85\ \mathrm{ps}^{-1}$ between two heavy-hole excitons of opposite spin was extracted from the $(\sigma^+\sigma^-\sigma^+)$ trace at the XX_h transition. Dephasing rates $\gamma_{63}=\gamma_{72}=1.2\ \mathrm{ps}^{-1}$ between heavy and light-hole excitons with op-

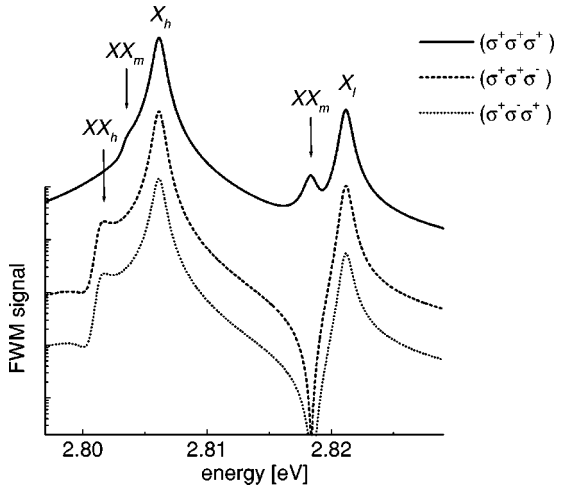

FIG. 5. Calculated FWM spectra into $\mathbf{k}_3+\mathbf{k}_2-\mathbf{k}_1$ direction for polarization configurations $(\sigma^+\sigma^+\sigma^+)$, $(\sigma^+\sigma^+\sigma^-)$, and $(\sigma^+\sigma^-\sigma^+)$ for the same conditions as in Fig. 1.

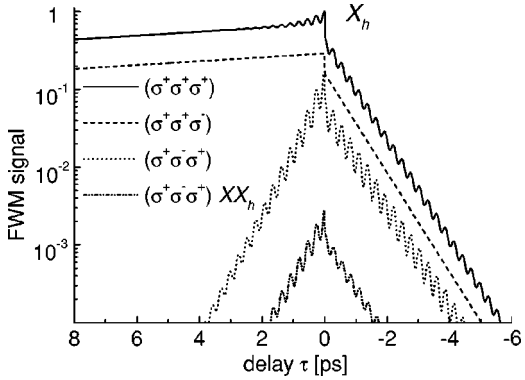

FIG. 6. Calculated FWM traces into $\mathbf{k}_3+\mathbf{k}_2-\mathbf{k}_1$ direction at the energetic position of the heavy-hole X_h exciton transition for configurations $(\sigma^+\sigma^+\sigma^+)$, $(\sigma^+\sigma^+\sigma^-)$, and $(\sigma^+\sigma^-\sigma^+)$ and at the biexciton induced transition XX_h for configuration $(\sigma^+\sigma^-\sigma^+)$ for the same conditions as in Fig. 2.

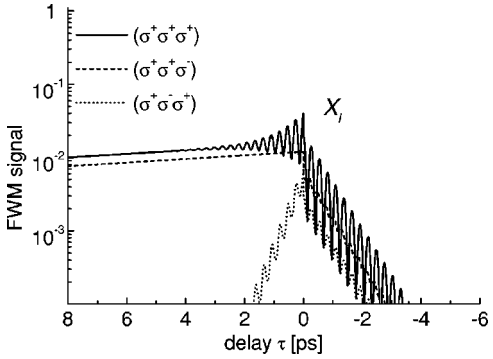

FIG. 7. Calculated FWM traces into the $\mathbf{k}_3+\mathbf{k}_2-\mathbf{k}_1$ direction at the energetic position of the light-hole X_l exciton transition for configurations $(\sigma^+\sigma^+\sigma^+)$, $(\sigma^+\sigma^+\sigma^-)$, and $(\sigma^+\sigma^-\sigma^+)$ for the same conditions as in Fig. 3.

posite spin were approximated from the $(\sigma^+\sigma^-\sigma^+)$ FWM trace at the XX_l transition. We assumed the same dephasing rates between heavy and light-hole excitons with equal spin e.g., $\gamma_{62}=\gamma_{73}=1.2\ \mathrm{ps}^{-1}$. For simplicity we further assumed that the dephasing rates γ_{ts} between two-exciton and single exciton states are equal to γ_{21}. The magnitude of the ground to heavy-hole dipole matrix elements $\mu_{21}=\mu_{31}$ and that of the ground to light-hole exciton dipole matrix elements $\mu_{61}=\mu_{71}$ were set to 1 and 0.57, respectively, according to their relative oscillator strength-ratios $\mu_{21}^2:\mu_{71}^2$ of 3:1 in relation to their valence band functions. Furthermore the spectral shape of the excitation pulse was considered as described in Ref. 9. The exciton–exciton scattering parameter β was determined from intensity dependent measurements to $\beta=22\ \mathrm{s}^{-1}\,\mathrm{cm}^2$ as outlined in the following paragraph. The still unknown parameters N, γ_{67}, and μ_{ts} were fitted to $N=2.8\cdot 10^{10}\ \mathrm{cm}^{-2}$, $\gamma_{76}=1.2\ \mathrm{ps}^{-1}$, and $\mu_{ts}=0.3$ for all two-exciton transitions to give reasonable agreement between experimental data and calculated spectra and traces.

As demonstrated in Fig. 5 the calculated FWM spectra for configurations $(\sigma^+\sigma^+\sigma^+)$, $(\sigma^+\sigma^+\sigma^-)$, and $(\sigma^+\sigma^-\sigma^+)$ at a delay time $\tau=-0.55$ ps reveal the same polarization dependence as observed in the experimental spectra shown in Fig. 1. In addition the relative signal intensities between the different exciton and biexciton transitions as well as between different polarization configurations are well reproduced.

The calculated FWM traces at the heavy-hole exciton transition X_h and at XX_h are shown in Fig. 6. According to the theoretical expression for the $(\sigma^+\sigma^+\sigma^+)$ configuration at $\tau>0$ the slow signal decay at long delay times is determined by the combined lifetime T_c. Occurring oscillations close to zero delay are generated by a term containing an exponential function $\exp(i\Omega_{62}^*\tau)$ and (weaker) by EID terms containing X_h and X_l transitions. The complex frequency $\Omega_{62}^*=\omega_{62}+i\,\gamma_{62}$ indicates the coherence between σ^+-X_h and σ^+-X_l excitons with a beating frequency of ω_{62}. Dephasing rate γ_{62} is responsible for the observed damping of the beats. The rise of the FWM intensity near zero delay is caused by EID since pulses $\mathbf{k}_1$ and $\mathbf{k}_3$ create an exciton grating so that the $\mathbf{k}_2$ exciton polarization is diffracted into direction $\mathbf{k}_3+\mathbf{k}_2-\mathbf{k}_1$. The contributing terms for $\tau<0$ at resonance ω_{21} contain the exponential functions $\exp(i\Omega_{21}\tau)$ and $\exp(i\Omega_{61}\tau)$, leading to the appearance of X_h-X_l quantum beats. Since dephasing rates γ_{21} and γ_{61} were chosen equal the FWM trace shows a single exponential decay and a constant oscillation amplitude with delay τ in agreement to the experimental observation.

In $(\sigma^+\sigma^+\sigma^-)$ configuration for delay $\tau>0$ the calculated FWM polarization is again governed by the exponential function $\exp(-\tau/T_1)$. There is no term accounting for quantum beats at resonance ω_{31}. Since the polarization directions are opposite for pulses $\mathbf{k}_1$ and $\mathbf{k}_3$ EID is inactive for pulse $\mathbf{k}_2$. Hence no EID signal close to zero delay is generated in agreement to the experimental observation. In contrast local field effects (LFE) arising from pulses $\mathbf{k}_2$ and $\mathbf{k}_1$ are active in $(\sigma^+\sigma^+\sigma^-)$ configuration and can lead to an additional FWM signal close to zero delay.[20] Since we do not observe a noticeable signal increase in our experiments we conclude that local field effects are of minor importance in consistence to our previous investigation.[19] The contributing terms for $\tau<0$ at resonance X_h contain only an exponential function $\exp(i\Omega_{31}\tau)$, explaining the lack of X_h-X_l quantum beats in this polarization configuration.

In $(\sigma^+\sigma^-\sigma^+)$ polarization configuration for $\tau>0$ the calculated FWM polarization at resonance ω_{31} is determined by terms containing exponents $\exp(-i\Omega_{32}\tau)$ and $\exp(i\Omega_{63}^*\tau)$ as well as EID (with dephasing rate 2 γ_{21}), thus leading to a multiexponential decay of the FWM signal and a damping of the X_h-X_l oscillation amplitude. In contrast the FWM polarization at the XX_h is generated by a term containing only the exponent $\exp(-i\Omega_{32}\tau)$. As mentioned earlier EID is inactive at transition XX_h. For $\tau<0$ the leading terms at resonance X_h contain the exponential functions $\exp(i\Omega_{21}\tau)$ and $\exp(i\Omega_{61}\tau)$, explaining the appearance of X_h-X_l quantum beats.

The calculated FWM traces at the energetic position of the light-hole exciton transition X_l are demonstrated in Fig. 7. The traces for $(\sigma^+\sigma^+\sigma^+)$, $(\sigma^+\sigma^+\sigma^-)$ configuration are very similar to the traces calculated at the X_h resonance and can be explained in a similar way. In polarization configuration $(\sigma^+\sigma^-\sigma^+)$ for $\tau>0$ the calculated FWM polarization

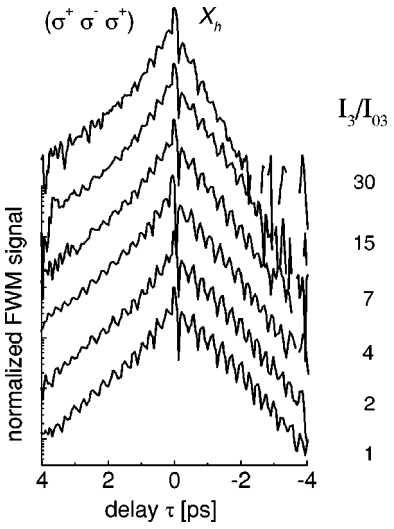

FIG. 8. Normalized FWM traces into $\mathbf{k}_3+\mathbf{k}_2-\mathbf{k}_1$ direction for the $(\sigma^+\sigma^-\sigma^+)$ configuration at the X_h exciton transition for a fixed $\mathbf{k}_1$ and $\mathbf{k}_2$ pulse intensity of 1.3 MW cm^{-2} and variable $\mathbf{k}_3$ pulse intensity labeled as ratio I_3/I_{03}. The $\mathbf{k}_3$ reference intensity is $I_{03}=0.6$ MW cm^{-2}, temperature was 55 K.

at resonance X_l is determined by terms containing exponential functions $\exp(-i\Omega_{72}\tau)$, $\exp(-i\Omega_{76}\tau)$ and by EID terms. Due to the larger dipole moments the magnitude of the $\exp(-i\Omega_{72}\tau)$ term is significantly larger than that of the $\exp(-i\Omega_{76}\tau)$ term so that an exact determination of the interexciton rate γ_{76} from the experimental data is very difficult. However, the experimental trace can be modeled consistently assuming $\gamma_{76}=\gamma_{72}$.

INTENSITY-DEPENDENT MEASUREMENTS

Despite some deviations from experimental results as e.g., the weaker FWM signal in the $(\sigma^+\sigma^+\sigma^-)$ configuration for $\tau>0$ or the stronger X_h–X_l beating in the $(\sigma^+\sigma^+\sigma^+)$ configuration for $\tau<0$, the model calculations successfully reproduce the experimental data and significantly contribute to the understanding of the complex FWM processes. In comparison with theory the experiments also provide reliable values for the interband dephasing rate $\gamma_{21}(N_3)$ as well as for the interexciton dephasing rates $\gamma_{32}(N_1+N_2)$ and $\gamma_{72}(N_1+N_2)$. However, since these values are obtained at different exciton densities a direct comparison between these dephasing rates is not admissible.

We therefore performed intensity dependent measurements in $(\sigma^+\sigma^-\sigma^+)$ configuration using the same experimental setup. In the first measurement series the intensity of pulses $\mathbf{k}_1$ and $\mathbf{k}_2$ was kept constant at 1.3 MW cm^{-2} and the intensity of the third pulse $\mathbf{k}_3$ was varied. In the second series the intensity of pulse $\mathbf{k}_3$ was kept constant at 0.3 MW cm^{-2} and the intensities of pulses $\mathbf{k}_1$ and $\mathbf{k}_2$ were varied. These measurements enable us to determine the dephasing rates $\gamma_{21}^0, \gamma_{32}^0, \gamma_{72}^0$ at zero exciton density and provide values for the exciton–exciton scattering parameters β_{21}, β_{32}, and β_{72}.

Figure 8 shows the normalized FWM traces for

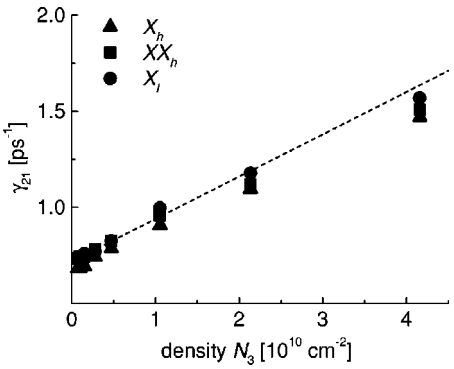

FIG. 9. Measured dephasing rates from FWM traces at the X_h, XX_h, and X_l transition energy as a function of the exciton density N_3 generated by pulse $\mathbf{k}_3$. The dashed line gives a linear increase of the dephasing rate γ_{21} with an exciton–exciton scattering parameter of $\beta_{21}=22$ s^{-1} cm^2.

$(\sigma^+\sigma^-\sigma^+)$ configuration at position X_h. The varied intensity of the third pulse $\mathbf{k}_3$ is specified as ratio I_3/I_{03} with respect to a reference intensity $I_{03}=0.6$ MW cm^{-2}. For $\tau<0$ pulse $\mathbf{k}_3$ arrives first so that exciton density N_3 is responsible for the density dependent dephasing of the nonlinear response according to $\gamma_{21}(N_3)=\gamma_{21}^0+\beta_{21}N_3$. For $\tau>0$ the decay rate $\gamma_{32}(N_1+N_2)$ of the FWM polarization remains nearly constant since the exciton density created by pulses $\mathbf{k}_1$ and $\mathbf{k}_2$ is constant. The observed increase of the FWM signal close to zero delay is attributed to higher order FWM processes which are not further discussed in this context.

Figure 9 depicts the extracted dephasing rates $\gamma_{21}(N_3)$ as a function of the exciton density N_3. The two-dimensional exciton density created by an excitation pulse with intensity 1 MW/cm^2 was estimated to $2.5\cdot10^9$ cm^{-2}.[9,19] Up to an exciton density of $N_3=2\cdot10^{10}$ cm^{-2} we find a linear dependence of dephasing rate $\gamma_{21}(N_3)$ in accordance to an exciton–exciton scattering parameter $\beta_{21}\approx22$ s^{-1} cm^2. Above $N_3=2\cdot10^{10}$ cm^{-2} the density dependence begins to saturate due to bleaching which is in agreement with FWM experiments performed on GaAs quantum wells at high excitation intensities.[25] Finally, a dephasing rate γ_{21}^0 was extrapolated to $\gamma_{21}^0=0.73$ ps^{-1}. Figure 9 also includes the dephasing rates obtained from traces at position XX_h and X_l. They reveal similar density dependence in particular nearly equal zero-density dephasing rates $\gamma_{21}^0\approx\gamma_{61}^0$ as well as equivalent exciton–exciton scattering parameters $\beta_{21}\approx\beta_{61}$ for X_h and X_l exciton transitions. The same scattering parameters $\beta_{21}\approx\beta_{61}$ and zero density rates $\gamma_{21}^0\approx\gamma_{61}^0$ are found if the constant $\mathbf{k}_1$ and $\mathbf{k}_2$ intensities are changed in these experiments.

Figure 10 shows normalized FWM traces for configuration $(\sigma^+\sigma^-\sigma^+)$ varying the intensity of $\mathbf{k}_1$ and $\mathbf{k}_2$ with $I_{01}+I_{02}=0.7$ MW cm^{-2} being the reference intensity for the different traces. In this situation the dephasing rate of the FWM signal remains constant for $\tau<0$ (constant exciton density N_3) while the dephasing rate for $\tau>0$ increases with increasing intensities of pulses $\mathbf{k}_1$ and $\mathbf{k}_2$. Deviations from this behavior are again attributed to $\chi^{(5)}$ and higher order

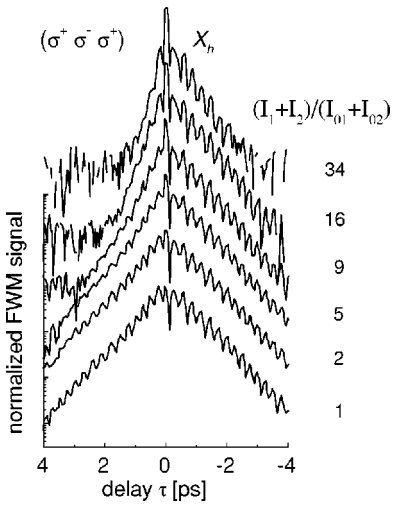

FIG. 10. Normalized FWM traces into the $\mathbf{k}_3+\mathbf{k}_2-\mathbf{k}_1$ direction for the $(\sigma^+\sigma^-\sigma^+)$ configuration at the X_h exciton transition for a fixed $\mathbf{k}_3$ pulse intensity of 0.3 MW cm^{-2} and variable $\mathbf{k}_1$ and $\mathbf{k}_2$ pulse intensity labeled as ratio $(I_1+I_2)/(I_{01}+I_{02})$. The $\mathbf{k}_1$ and $\mathbf{k}_2$ reference intensity is $I_{01}+I_{02}=0.7$ MW cm^{-2}, temperature was 55 K.

effects. Figure 11 depicts the extracted dephasing times at spectral positions X_h and XX_h. At position X_h the extracted values represent an average dephasing rate involving the dephasing rates γ_{32} (dominating term), γ_{63} and 2 γ_{21} (from EID). The rate at position XX_h only accounts for the interexciton dephasing rate γ_{32} and is therefore somewhat lower as compared to the average value obtained from the X_h trace. In linear approximation the density dependence of dephasing rate γ_{32} is given by $\gamma_{32}(N_1+N_2)=\gamma_{32}^0+\beta_{32}(N_1+N_2)$. Up to a density of $N_1+N_2\approx 2\cdot 10^{10}$ cm^{-2} we find a linear increase of γ_{32} in accordance to an exciton–exciton scattering parameter $\beta_{32}\approx 22$ s^{-1} cm^2 indicating the same Coulomb scattering efficiency for heavy-hole interband and interexciton coherences. Above density $N_1+N_2=2\cdot 10^{10}$ cm^{-2} the dependence starts to saturate as already observed in the measurements before. The zero-density dephasing rate γ_{32}^0 was

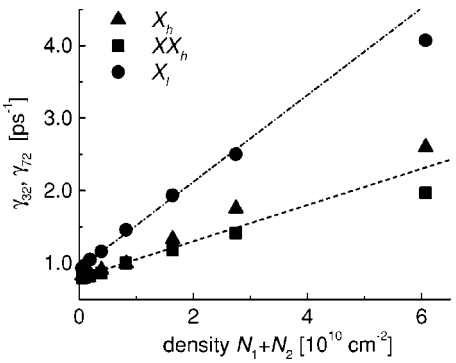

FIG. 11. Measured dephasing rates from FWM traces at the X_h, XX_h, and X_l transition energy as a function of the exciton density N_1+N_2 generated by pulses $\mathbf{k}_1$ and $\mathbf{k}_2$. The dashed and dotted–dashed lines give a linear increase of the dephasing rate γ_{32} and γ_{72} with scattering parameter $\beta_{32}=22$ s^{-1} cm^2 and $\beta_{72}=60$ s^{-1} cm^2, respectively.

determined to $\gamma_{32}^0=0.8$ ps^{-1} indicating similar exciton-phonon and exciton-impurity scattering mechanisms for both types of coherences. The same scattering parameter β_{32} and zero density rate γ_{32}^0 are found if the constant $\mathbf{k}_3$ intensity is changed in these experiments.

Figure 11 also contains dephasing rates which have been extracted from the FWM trace at the spectral position of X_l. From similar arguments as at position X_h the extracted rates are average values between rates γ_{72} and 2 γ_{21}. The contribution of the γ_{76} containing term can be neglected due to its weak dipole matrix elements. In comparison with our model calculations we estimate an exciton–exciton scattering parameter of $\beta_{72}\geqslant 60$ s^{-1} cm^2. This significantly stronger exciton–exciton interaction for the X_h–X_l interexciton coherence as compared to the X_h–X_h coherence is also noticeable in Fig. 10 by the increasing damping of the X_h–X_l oscillations with rising exciton density. Finally, the zero-density rate γ_{72}^0 is estimated to $\gamma_{72}^0=0.9$ ps^{-1} indicating similar exciton-phonon or exciton-impurity interactions for all coherences. The enhanced exciton–exciton scattering of rate β_{72} might be explained by an increased Pauli repulsion between σ^+ X_h–σ^- X_l coherences and σ^+ X_h excitons (or between σ^- X_h–σ^+ X_l coherences and σ^- X_h excitons), where all interacting excitons carry electrons of equal spin momentum $m_s=-1/2$ (or $m_s=+1/2$, respectively).

Although an evaluation of the interexciton dephasing γ_{76} is not feasible from our experiment we may expect that the zero-density dephasing rate γ_{76}^0 is similar to γ_{32}^0. Since only two electrons of equal spin momentum are involved in X_l–X_l coherence scattering events (same as for the X_h–X_h interexciton coherence) we might further conclude that the exciton–exciton scattering parameter β_{76} is smaller than that of the X_h–X_l coherence. Further spectrally resolved three-pulse FWM experiments using spectrally narrow 1 ps pulses for individual excitation of either X_h or X_l exciton transitions may help to clarify this assumption.

CONCLUSIONS

We have performed spectrally resolved and polarization dependent three-pulse FWM experiments to study the interband (γ_{21}, γ_{61}) and interexciton dephasing rates (γ_{32}, γ_{72}) in a homogeneously broadened ZnSe/$Zn_{0.90}Mg_{0.1}Se$ single quantum well. The characteristic features of the experimental FWM spectra and traces have been successfully reproduced by calculations based on extended optical Bloch equations for a 10-level system. In particular we find a significant EID contribution from its polarization dependence. Intensity dependent three-pulse FWM measurements show that the zero-density dephasing rate of X_h and X_l interband coherences ($\gamma_{21}^0=\gamma_{61}^0=0.73$ ps^{-1}) is nearly equal to that of the interexciton coherence between two X_h excitons ($\gamma_{32}^0=0.8$ ps^{-1}) and between X_h–X_l excitons ($\gamma_{72}^0=0.9$ ps^{-1}) of opposite spin. This result indicates similar exciton-phonon and exciton-impurity interaction for all types of coherences. In addition the Coulomb scattering for interband excitons ($\beta_{21}\approx 22$ s^{-1} cm^2) and that for the interexciton X_h–X_h coherence ($\beta_{32}\approx 22$ s^{-1} cm^2) is found to be equal while the inter-

exciton $X_h - X_l$ coherence shows a significant higher scattering rate ($\beta_{72} \approx 60\ s^{-1}\ cm^2$). The enhancement for the $X_h - X_l$ coherence is attributed to an increased Pauli repulsion in scattering events where three electrons of equal spin momentum are involved.

ACKNOWLEDGMENTS

The experimental support of H. P. Tranitz is kindly acknowledged. This work is supported by the National Science Foundation (DMR-0305076).

[1] D. Bennhardt, P. Thomas, R. Eccleston, K. J. Mayer, and J. Kuhl, Phys. Rev. B **47**, 13485 (1993).
[2] E. J. Mayer, G. O. Smith, V. Heuckeroth, J. Kuhl, K. Bott, A. Schulze, T. Meier, S. W. Koch, P. Thomas, R. Hey, and K. Ploog, Phys. Rev. B **51**, 10909 (1995).
[3] J. Erland, D. Birkedal, V. G. Lyssenko, and J. M. Hvam, J. Opt. Soc. Am. B **13**, 981 (1996).
[4] L. Schultheis, A. Honold, J. Kuhl, and C. W. Tu, Phys. Rev. B **34**, 9027 (1986).
[5] D.-S. Kim, J. Shah, J. E. Cunningham, T. C. Damen, S. Schmitt-Rink, and W. Schäfer, Phys. Rev. Lett. **68**, 2838 (1992).
[6] A. Honold, L. Schultheis, J. Kuhl, and C. W. Tu, Phys. Rev. B **40**, 6442 (1989).
[7] R. Hellmann, M. Koch, J. Feldmann, S. T. Cundiff, E. O. Göbel, D. R. Yakovlev, A. Waag, and G. Landwehr, J. Cryst. Growth **138**, 791 (1994).
[8] A. J. Fischer, D. S. Kim, J. Hays, W. Sham, J. J. Song, D. B. Eason, J. Ren, J. F. Schetzina, H. Luo, and J. K. Furdyna, Phys. Rev. B **50**, 17643 (1994).
[9] H. P. Wagner, A. Schätz, R. Maier, W. Langbein, and J. M. Hvam, Phys. Rev. B **57**, 1791 (1998).
[10] L. Schultheis, A. Honold, J. Kuhn, J. Köhler, and C. W. Tu, Phys. Rev. B **34**, 9027 (1986).
[11] A. J. Fischer, D. S. Kim, J. Hays, W. Shan, J. J. Song, D. B. Eason, J. Ren, J. F. Schetzina, H. Luo, J. K. Furdyna, Z. Q. Zhu, T. Yao, J. F. Kiem, and W. Schäfer, Phys. Rev. Lett. **73**, 2368 (1994).
[12] M. Lindberg and S. W. Koch, Phys. Rev. B **38**, 3342 (1988).
[13] M. Wegener, D. S. Chemla, S. Schmitt-Rink, and W. Schäfer, Phys. Rev. A **42**, 5675 (1990).
[14] Y. Z. Hu, R. Binder, S. W. Koch, S. T. Cundiff, H. Wang, and D. G. Steel, Phys. Rev. B **49**, 14382 (1994).
[15] H. Wang, K. Ferrio, D. G. Steel, Y. Z. Hu, R. Binder, and S. W. Koch, Phys. Rev. Lett. **71**, 1261 (1993).
[16] H. Wang, K. B. Ferrio, D. G. Steel, P. R. Berman, Y. Z. Hu, R. Binder, and S. W. Koch, Phys. Rev. A **49**, R1551 (1994).
[17] H. Wang, J. Shah, T. C. Damen, and L. N. Pfeiffer, Solid State Commun. **91**, 869 (1994).
[18] E. J. Mayer, G. O. Smith, V. Heuckeroth, J. Kuhl, K. Bott, A. Schulze, T. Mayer, D. Bennhardt, S. W. Koch, P. Thomas, B. Hey, and K. Ploog, Phys. Rev. B **50**, 14730 (1994).
[19] H. P. Wagner, W. Langbein, J. M. Hvam, and Arthur L. Smirl, Phys. Rev. B **60**, 4454 (1999).
[20] G. O. Smith, E. J. Mayer, V. Heuckeroth, J. Kuhl, K. Bott, T. Meier, A. Schulze, and D. Bennhardt, Solid State Commun. **94**, 373 (1995).
[21] K. Bott, E. J. Mayer, G. O. Smith, V. Heuckeroth, M. Huebner, J. Kuhl, T. Maier, A. Schulze, M. Lindberg, S. W. Koch, P. Thomas, R. Hey, and K. Ploog, J. Opt. Soc. Am. B **13**, 1026 (1996).
[22] H. P. Wagner, W. Langbein, and J. M. Hvam, Phys. Rev. B **59**, 4584 (1999).
[23] M. Wörz, E. Griebl, Th. Reisinger, B. Flierl, D. Haserer, T. Semmler, T. Frey, and W. Gebhardt, Phys. Status Solidi B **202**, 805 (1997).
[24] J. Erland, B. S. Razbirin, K.-H. Pantke, V. G. Lyssenko, and J. M. Hvam, Phys. Rev. B **47**, 3582 (1993).
[25] B. Pal and A. S. Vengurlekar, Phys. Rev. B **66**, 155337 (2002).